EJMS

European Journal of Mass Spectrometry
2019, Vol. 25(1) 16–29

DOI: 10.1177/1469066718798097
journals.sagepub.com/home/ems
SAGE

Relative glycosidic bond stabilities of naturally occurring methylguanosines: 7-methylation is intrinsically activating

Zachary J Devereaux, Y Zhu and MT Rodgers

Abstract

The frequency and diversity of posttranscriptional modifications add an additional layer of chemical complexity beyond canonical nucleic acid sequence. Methylations are particularly frequently occurring and often highly conserved throughout the kingdoms of life. However, the intricate functions of these modified nucleic acid constituents are often not fully understood. Systematic foundational research that reduces systems to their minimum constituents may aid in unraveling the complexities of nucleic acid biochemistry. Here, we examine the relative intrinsic *N*-glycosidic bond stabilities of guanosine and five naturally occurring methylguanosines (O2′-, 1-, 7-, N2,N2-di-, and N2,N2,O2′-trimethylguanosine) probed by energy-resolved collision-induced dissociation tandem mass spectrometry and complemented with quantum chemical calculations. Apparent glycosidic bond stability is generally found to increase with increasing methyl substitution (canonical < mono- < di- < trimethylated). Many biochemical transformations, including base excision repair mechanisms, involve protonation and/or noncovalent interactions to increase nucleobase leaving-group ability. The protonated gas-phase methylguanosines require less activation energy for glycosidic bond cleavage than their sodium cationized forms. However, methylation at the N7 position intrinsically weakens the glycosidic bond of 7-methylguanosine more significantly than subsequent cationization, and thus 7-methylguanosine is suggested to be under perpetually activated conditions. N7 methylation also alters the nucleoside geometric preferences relative to the other systems, including the nucleobase orientation in the neutral form, sugar puckering in the protonated form, and the preferred protonation and sodium cation binding sites. All of the methylated guanosines examined here are predicted to have proton affinities and gas-phase basicities that exceed that of canonical guanosine. Additionally, the proton affinity and gas-phase basicity trends exhibit a roughly inverse correlation with the apparent glycosidic bond stabilities.

Keywords

Nucleic acid modifications, 7-methylguanosine, 2′-O-methylguanosine, energy-resolved collision-induced dissociation, glycosidic bond stability, glycosidic bond activation, quadrupole ion trap mass spectrometry, survival yield analysis, density functional theory calculations, proton affinity

Received 18 June 2018; accepted 10 August 2018

Introduction

The diverse biochemical functions of ribonucleic acid (RNA) necessitate extensive, precise, and flexible intramolecular and intermolecular interactions with various nucleic acid strands, enzymes, and protein cofactors. Accordingly, RNA strands generally undergo various processing steps after transcription, including extensive modifications to their canonical nucleoside constituents, which contribute to the biochemical complexity affording their unique and diversified qualities.[1–5] Methylations are among the most common nucleic acid modifications and are crucially produced in all three phylogenetic kingdoms (eukarya, bacteria, and archaea) at a variety of atom positions.[6–12] There are now at least 163 reported RNA constituent modifications; of these, approximately two-thirds include methylations.[13,14] Among the 20 reported naturally modified forms of guanosine (Guo), simple

Department of Chemistry, Wayne State University, Detroit, USA

This article is dedicated to Robert C. Dunbar, a great friend, colleague, and scientist, and in appreciation for his many contributions to gas-phase ion chemistry and spectroscopy.

Corresponding author:
MT Rodgers, Department of Chemistry, Wayne State University, 5101 Cass Avenue, Detroit, MI 48202, USA.
Email: mrodgers@chem.wayne.edu

methylations comprise 11 of them.[15,16] RNA methylations generally contribute to secondary and tertiary structure formation and stability as well as site-specific recognition and interaction by adding steric bulk, blocking canonical base-pairing interactions, and creating additional hydrophobic effects.[17] Methylations are also implicated in stabilizing RNA structures in response to heat shock,[18] including in extreme thermophile archaebacteria.[5,19–23] Additionally, methylations can be reversible and dynamically controlled for biological regulatory purposes, including control over the circadian clock.[24–26]

Guo, one of the four canonical RNA nucleosides, is composed of the purine nucleobase guanine (Gua) attached to a ribose sugar via an *N*-glycosidic linkage. The complementary DNA nucleoside, 2′-deoxyguanosine (dGuo), is formed by linking Gua and 2′-deoxyribose. The covalent glycosidic linkages between nucleobases and their constituent sugars retain the nucleic acid sequence and genetic information fidelity. O2′-Methylation is one of the most common natural RNA modifications. The locations of most O2′-methylations on vertebrate ribosomes are highly conserved, suggesting they have necessary and phylogenetically conserved functions.[27,28] The virulence of RNA viruses is enhanced with O2′-methylated 5′-cap structures, a specially modified region that is also essential in stabilizing mature messenger RNA (mRNA), by aiding evasion of cellular defense mechanisms through increased enzyme–substrate interaction specificity.[29] O2′-methylguanosine (Guom) is one such nucleoside. Increased Guom biosynthesis was observed in a thermally stressed extreme thermophile, reinforcing its association with RNA thermal stability.[22] 1-Methylguanosine (m^1Guo) is conserved at positions 9 and 37 of the 3′-end of transfer RNA (tRNA) anticodons in all three biologic kingdoms where it aids in prevention of translational frameshifting.[30–32] The intrinsically methyl cationized 7-methylguanosine (m^7Guo) persistently appears at the 5′-cap of eukaryotic mRNA[33] where it provides vital protection from degradation and allows efficient recognition and translation on the ribosome.[34,35] Recognition and complexation specificity is enhanced in this region by O2′-methylations of the first few nucleosides immediately following the triphosphate linkage of m^7Guo with the penultimate nucleoside.[36] N2,N2-Dimethylguanosine ($m^2{}_2$Guo) is highly conserved at position 26 of tRNA, and its presence is correlated with the formation of certain atypical tRNA structures.[37–40] N2,N2,O2′-trimethylguanosine ($m^2{}_2$Guom) is a nucleoside unique to thermophilic archaebacteria tRNA that is thought to stabilize stacking interactions against thermal motion.[20,21,23]

Methylations can also be forms of nucleic acid damage.[41] Undesirable alkylations are either degraded or repaired. Repairs occur through various biochemical mechanisms, such as oxidative demethylation and base excision repair (BER).[24,42,43] Enzymatic BER pathways involve complete removal and replacement of the undesired nucleobase through controlled hydrolytic glycosidic bond cleavages. There is much experimental and theoretical evidence suggesting that biological BER mechanisms involve both stepwise S_N1 and concerted S_N2 substitution reactions that are initialized by enhancing the purine nucleobase leaving-group ability via protonation.[44–48] Solution-based studies also show that increased acid concentration alone increases glycosidic bond hydrolysis rates of the dissolved purine nucleosides Guo, dGuo, 2′-deoxyadenosine (dAdo), m^7Guo, and 7-methyl-2′-deoxyguanosine (m^7dGuo).[49]

Despite the vast knowledge of nucleic acids currently amassed, the complex, dynamic, and critical roles modifications play in cellular processes are still incompletely understood. Tandem mass spectrometry (MS/MS) approaches have proven effective in providing insight into the intrinsic properties of nucleic acid constituents. Performing collision-induced dissociation (CID) in an energy-resolved fashion has also proved useful for a variety of purposes including the separation of isobaric compounds,[50] nucleic acid constituent proton affinity (PA) measurements,[51] relative stability measurements of canonical nucleosides,[52–56] glycosyl phosphates,[57] 9-ethylguanine tetrads,[58] nucleic acid–drug complexes,[59] and accurate absolute glycosidic bond cleavage thermochemistry measurements via threshold collision-induced dissociation (TCID).[60–63] Here we use energy-resolved collision-induced dissociation (ER-CID) MS/MS experiments performed in a quadrupole ion trap mass spectrometer (QIT MS) to elucidate the relative intrinsic *N*-glycosidic bond stabilities of the protonated and sodium cationized forms of canonical Guo and five methylguanosines (Guom, m^1Guo, m^7Guo, $m^2{}_2$Guo, and $m^2{}_2$Guom). Theoretical calculations on the neutral, protonated, and sodium cationized forms of these nucleosides (Nuo, $[Nuo+H]^+$, and $[Nuo+Na]^+$) are used to enhance and support interpretation of the experimental results.

Experimental

Materials and sample preparation

Guo and Guom were purchased from Alfa Aesar (Ward Hill, MA, USA). The remaining four methylguanosines (m^1Guo, m^7Guo, $m^2{}_2$Guo, and $m^2{}_2$Guom) were extracted from natural sources by the University of Utah Departments of Medicinal Chemistry and Biochemistry (Salt Lake City, UT, USA) and brought to the Wayne State University Department of Chemistry (Detroit, MI, USA) for analysis. Water and sodium chloride were purchased from Sigma-Aldrich (St Louis, MO, USA). Methanol was purchased from Fisher Scientific (Pittsburgh, PA, USA). Acetic acid was purchased from Mallinckrodt Chemicals (St Louis, MO, USA). All chemicals were used as received. Standard solutions were created for each nucleoside and diluted to concentrations of

~10 µM in 50/50 (v/v) methanol/water. To facilitate generation of the protonated nucleosides, these solutions were modified with ~1% (v/v) acetic acid. For the sodium cationized systems, ~10 µM sodium chloride was added to the nucleoside solutions.

Mass spectrometry and CID

Experiments were performed on an amaZon ETD QIT mass spectrometer (Bruker Corporation, Billerica, MA, USA; Bruker Daltonics, Bremen, Germany) equipped with an Apollo II electrospray ionization (ESI) source. Compass Data Analysis 4.0 software (Bruker Daltonics, Bremen, Germany) was used to acquire, extract, and export the mass spectral data. The individual nucleoside working standards were introduced to the atmospheric pressure ESI source at a flow rate of ~3 µl/min using a mechanical syringe pump. A voltage of ~4 kV was applied in the ESI source to aid in generation and extraction of ions into the inlet of the mass spectrometer. The nitrogen nebulizer gas pressure was set at 10 psi, while the nitrogen dry gas flow rate and temperature were set at 3 L/min and 200°C, respectively, to aid in desolvation. The generated ions were transferred through the differential region and ion guides, operated under mild conditions to avoid collisional activation of the ions, and into the QIT. A positive isolation voltage between the transfer optics and the QIT prevents additional accumulation of ions in the QIT while the scan sequence proceeds. After injection into the QIT, ion trajectories and internal energies were dampened and cooled through collisions with the neutral bath gases and the desired precursor ions were mass isolated. Helium present in the trap chamber at a stagnation pressure of ~1 mTorr was used as the CID collision gas. For CID, the adjustable auxiliary rf excitation amplitude was applied during a 40 ms activation window. After this activation window the primary trapping rf voltage was ramped, sequentially ejecting ions of increasing mass-to-charge ratio (m/z) from the QIT to the conversion dynode-based detector system. The low mass cutoff was set to 27% of the precursor ion mass in all experiments.

ER-CID and survival yield analysis

ER-CID experiments were performed on the protonated and sodium cationized forms of Guo, Guom, m^1Guo, m^7Guo, $m^2{}_2$Guo, and $m^2{}_2$Guom (see Figure 1). ER-CID data and analysis of $[Guo+H]^+$ and $[Guo+Na]^+$ were previously published[52] in relation to $[dGuo+H]^+$ and $[dGuo+Na]^+$ and is included here for comparisons with the methylguanosines. In the experiments herein, mass spectra were continuously acquired while the auxiliary rf excitation amplitude, applied during the activation window, was ramped from 0.00 V to a value beyond that required to achieve 100% precursor ion dissociation (0.60 V maximum for the systems examined here) in steps of 0.01 V per 30 s

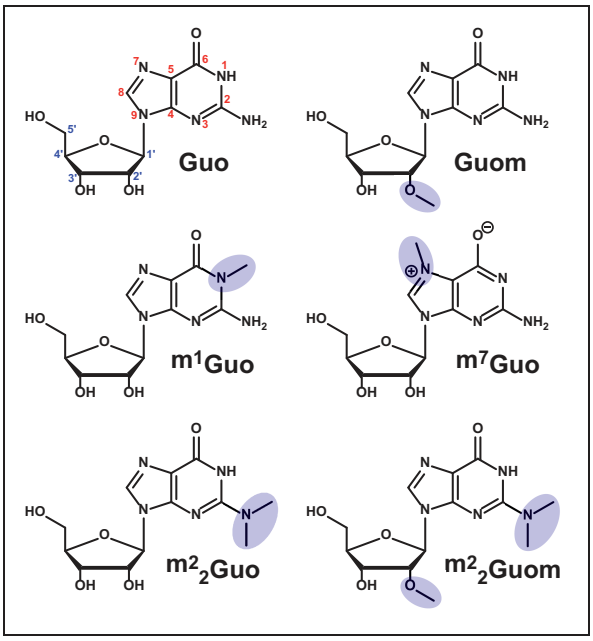

Figure 1. Neutral forms of guanosine (Guo), O2′-methylguanosine (Guom), 1-methylguanosine (m^1Guo), 7-methylguanosine (m^7Guo), N2,N2-dimethylguanosine ($m^2{}_2$Guo), and N2,N2,O2′-trimethylguanosine ($m^2{}_2$Guom). Methylation sites of the modified nucleosides are highlighted in blue. The atom numbering scheme is displayed on Guo. Note the zwitterionic character of m^7Guo.

increments. With the experimental sequence employed ~50 mass spectra were collected and averaged at each rf excitation amplitude during each trial. ER-CID experiments were performed in triplicate. Custom software developed in our laboratory was used to extract raw intensity data from the Bruker data files and calculate survival yields according to equation (1)

$$Survival\ Yield = I_p/(I_p + I_f) \tag{1}$$

where I_p is the precursor ion intensity and I_f is the total fragment ion intensity. Survival yields were plotted as a function of applied rf excitation amplitude.

Survival yield data were fit with a four-parameter logistic dynamic curve of the form found in equation (2)

$$Survival\ Yield = min + \frac{max - min}{1 + \left(\frac{rf_{EA}}{\mathrm{CID}_{50\ \%}}\right)^{CIDslope}} \tag{2}$$

where *max* and *min* are adjustable maximum and minimum parameters, respectively, set to 1 (100% survival yield) and 0 (0% survival yield) as appropriate for this work, rf_{EA} is the rf excitation amplitude applied in the CID experiment, $\mathrm{CID}_{50\%}$ is the rf excitation amplitude required to give a *Survival Yield* of 50%, and *CIDslope* is the slope of the declining region of the survival yield curve. The $\mathrm{CID}_{50\%}$ is extracted from this fit and used as a relative measure of the *N*-glycosidic bond stabilities of $[Nuo+H]^+$ and $[Nuo+Na]^+$. SigmaPlot Version 10.0

(Systat Software, Inc., San Jose, CA, USA) was used to fit, analyze, and plot the data.

Theoretical calculations

Structures of the neutral nucleosides and all potentially favorable proton and cation binding modes of the protonated and sodium cationized forms of the nucleosides studied here (Guo, Guom, m^1Guo, m^7Guo, $m^2{}_2$Guo, and $m^2{}_2$Guom; Figure 1) were built. These systems were subjected to molecular mechanics simulated annealing procedures to produce a large and varied number of structural motifs that were further refined via quantum chemical calculations. Neutral Guo, $[Guo+H]^+$, and $[Guo+Na]^+$ conformers were calculated previously for infrared multiple photon dissociation (IRMPD) action spectroscopy studies[52,64]; these structures were used for comparisons here, and parallel computational methods were employed in the novel calculations performed in the current study.

The neutral structures were examined as they are constructed in Figure 1. The favorable protonation sites examined for Guo, Guom, m^1Guo, $m^2{}_2$Guo, and $m^2{}_2$Guom included the N3, O6, and N7 positions; in m^7Guo, the protonation sites examined included the N1, N3, and O6 atoms. Sodium cation binding modes were studied by explicitly binding the sodium to single heteroatoms and allowing them to relax into low-energy, generally multidentate, structures during the molecular mechanics simulations. The monodentate sodium cation binding sites considered included the N3, O6, N7, O2′, O3′, O4′, and O5′ atoms for Guo, Guom, m^1Guo, $m^2{}_2$Guo, and $m^2{}_2$Guom. The same binding sites were also considered for m^7Guo except that the N7 site was again exchanged for the N1 site.

Simulated annealing procedures were performed for each of the neutral nucleosides, as well as for each of the protonation sites and monodentate sodium cation binding sites for each nucleoside as described above. The Amber 3 force field and HyperChem software (HyperCube, Inc., Gainesville, FL, USA) were used. This procedure comprises heating from 0 to 1000 K over 0.3 ps, sampling conformational space at 1000 K for 0.2 ps, and cooling to 0 K over 0.3 ps. The resulting structures are then optimized to a local minimum, and a snapshot was saved and used to initiate the next simulated annealing cycle. This process was repeated 300 times for each initial structure of each nucleoside.

Select output from the simulated annealing procedure (generally the 30 lowest energy conformers) was subjected to density functional theory (DFT) calculations via the Gaussian 09 suite.[65] Geometry optimizations and frequency analyses were performed at the B3LYP/6-311+G(d,p) level of theory at standard ambient temperature and pressure and with a frequency scaling factor of 0.9887.[66] Single point energy calculations were performed at the B3LYP/6-311+G(2d,2p) level of theory. Conformations of interest were translated from one nucleoside form to the others by functional group modifications to the DFT optimized structure outputs. These modified structures were then subjected to the same DFT treatment.

Results

CID

The CID of the protonated and sodium cationized forms of Guo, Guom, m^1Guo, m^7Guo, $m^2{}_2$Guo, and $m^2{}_2$Guom (Figure 1) all proceed solely through cleavage of the C1′–N9 glycosidic bond. For all systems, the cation is solely retained by the nucleobase. This singular process was observed at all rf excitation amplitudes that produced fragmentation, i.e. no other dissociation channels were observed. The general CID reaction occurs as described in reaction (3)

$$[Nuo+C]^+ \overset{n\,He}{\rightarrow} [Base+C]^+ + (Nuo-Base) \quad (3)$$

where *Nuo* represents each of the nucleosides studied, *C* is the cationization agent (either a proton or sodium cation), *Base* is the corresponding nucleobase fragment, and (*Nuo*−*Base*) is the corresponding neutral sugar fragment (undetectable in the mass spectrometer). The protonated or sodium cationized nucleoside is cleaved at the glycosidic bond, a proton is abstracted from the sugar constituent by the nucleobase, and the nucleobase retains the original cationization agent. The neutral nucleoside and corresponding nucleobase names and abbreviations are given in Table 1, the m/z values of the precursor and fragment ions observed are listed in Table S1, mass spectra acquired at rf excitation amplitudes producing ~50% dissociation are displayed in Figure S1, and reaction schemes with proposed chemical structures are depicted in Figure S2. The structures of the neutral sugars shown in Figure S2 were not experimentally verified but are consistent with theoretical predictions.[61]

ER-CID and survival yield analysis

Survival yield as a function of rf excitation amplitude is plotted for the protonated (solid lines) and sodium cationized (dashed lines) forms of all six guanosine nucleosides in Figure 2. Expanded views of the data over the range of rf excitation amplitudes that produce dissociation are provided in Figure S3. The error bars represent one standard deviation of the measurements made in triplicate. The four-parameter logistic curve fits to the data take on their expected sigmoidal "S" shape. At low excitation energies (below the activation energy threshold) 100% of the precursor ions survive the activation process and the survival yield is unity. At specific collision energies characteristic to the precursor ion, the ions acquire sufficient internal energy to undergo dissociation (survival yield begins to deviate from 1), and the dissociation efficiency increases with increasing excitation amplitude ($0 < \text{survival yield} < 1$), until

Table 1. Nucleoside and corresponding nucleobase names and abbreviations.

Nucleoside (Nuo)		Nucleobase (Base)	
Name	Abbreviation	Name	Abbreviation
Guanosine	Guo	Guanine	Gua
1-Methylguanosine	m^1Guo	1-Methylguanine	m^1Gua
7-Methylguanosine	m^7Guo	7-Methylguanine	m^7Gua
O2′-Methylguanosine	Guom	Guanine	Gua
N2,N2-Dimethylguanosine	m^2_2Guo	N2,N2-Dimethylguanine	m^2_2Gua
N2,N2,O2′-Trimethylguanosine	m^2_2Guom	N2,N2-Dimethylguanine	m^2_2Gua

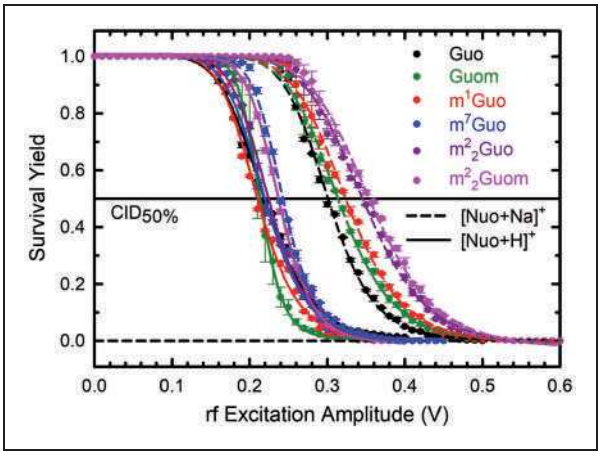

Figure 2. Survival yield curves for the protonated (solid lines) and sodium cationized (dashed lines) forms of guanosine and the methylguanosines. The data are color coded as indicated in the legend of the figure. The $CID_{50\%}$ line is shown in solid black, whereas complete precursor ion dissociation is indicated as a dashed black line. Survival yield results for Guo are taken from previous work.[52]

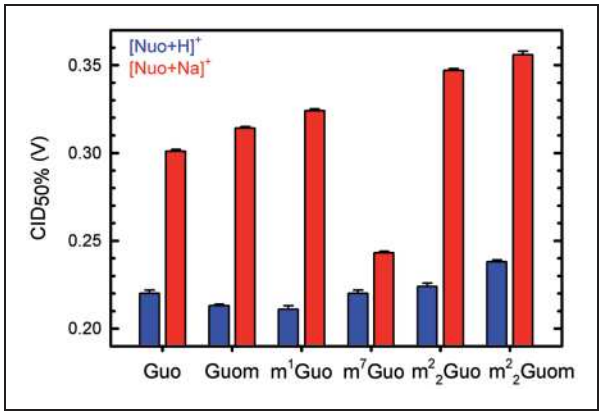

Figure 3. $CID_{50\%}$ values of the protonated (blue bars) and sodium cationized (red bars) forms of guanosine and the methylguanosines. The error bars correspond to the standard error of the survival yield curve fits.

finally 100% precursor ion dissociation is achieved (survival yield of 0). The $CID_{50\%}$ of each system is extracted from fits of the survival yield data and used as a measure of relative stability.

Because all CID reactions observed proceed through the same dissociation channel (*N*-glycosidic bond cleavage, Figures S1 and S2), the extracted $CID_{50\%}$ values (Figure 3 and Table S1) correlate with the relative energies required to activate the *N*-glycosidic bonds of these nucleoside ions. The $[Nuo+H]^+$ and $[Nuo+Na]^+$ data are displayed as blue and red bars, respectively. The error bars correspond to the standard error associated with the four-parameter logistic curve fit. The $CID_{50\%}$ (in Volts), and thus the apparent relative *N*-glycosidic bond stability, of the protonated systems increases in the following order: $[m^1Guo+H]^+$ $(0.211 \pm 0.002) <$ $[Guom+H]^+$ $(0.213 \pm 0.001) < [Guo+H]^+$ $(0.220 \pm 0.002) \approx [m^7Guo+H]^+$ $(0.220 \pm 0.002) < [m^2_2Guo+H]^+$ $(0.224 \pm 0.002) < [m^2_2Guom+H]^+$ (0.238 ± 0.001). For the sodium cationized nucleosides, the extracted $CID_{50\%}$ values (in Volts) increase in the following order: $[m^7Guo+Na]^+$ (0.243 ± 0.001) << $[Guo+Na]^+$ $(0.301 \pm 0.002) < [Guom+Na]^+$ $(0.314 \pm 0.001) < [m^1Guo+Na]^+$ $(0.324 \pm 0.001) < [m^2_2Guo+Na]^+$ $(0.347 \pm 0.001) < [m^2_2Guom+Na]^+$ (0.356 ± 0.002). The $CID_{50\%}$ values determined for the protonated forms of the nucleosides span a range of 0.027 V from 0.211 to 0.238 V. The $CID_{50\%}$ values determined for the sodium cationized forms span a much larger range of 0.113 V from 0.243 to 0.356 V when all six nucleoside complexes are included, but reduces to 0.055 V from 0.301 to 0.356 V when $[m^7Guo+Na]^+$ is excluded. The average $CID_{50\%}$ for the protonated nucleosides is 0.221 ± 0.010 V. The average $CID_{50\%}$ for all six sodium cationized forms is 0.314 ± 0.040 V and increases to 0.328 ± 0.023 V when $[m^7Guo+Na]^+$ is excluded. The $CID_{50\%}$ value determined for $[m^7Guo+Na]^+$ (0.243 ± 0.001) is much closer to the average value determined for the protonated nucleosides $(0.221 \pm 0.010, +0.022$ V difference) than the average determined for the other sodium cationized nucleosides $(0.328 \pm 0.023, -0.085$ V difference). Additionally, the protonated system with the $CID_{50\%}$ nearest to that of $[m^7Guo+Na]^+$ is $[m^2_2Guom+H]^+$ at 0.238 ± 0.001 (+0.005 V difference), whereas the nearest sodium cationized system is $[Guo+Na]^+$ at 0.301 ± 0.002 (−0.058 V difference).

The trends in the $CID_{50\%}$ values indicate that the *N*-glycosidic bonds of these nucleosides are generally more activated by protonation than sodium cationization (i.e. the protonated forms are intrinsically less stable than the sodium cationized forms). The major outlier from this trend is $[m^7Guo+Na]^+$ with a $CID_{50\%}$ that is closer to those of the protonated forms than the other sodium cationized forms, although it is still slightly greater (more stable) than that of the most stable protonated form $[m^2{}_2Guom+H]^+$. The trimethylated $m^2{}_2Guom$ exhibits the highest apparent *N*-glycosidic bond strength among the nucleosides studied, followed by the dimethylated $m^2{}_2Guo$, which exhibits the second highest apparent *N*-glycosidic bond strength.

Theoretical calculations: Guanine orientations and sugar puckerings

Features of the ground Nuo, $[Nuo+H]^+$, and $[Nuo+Na]^+$ conformers (Figure 4) are described and discussed in the main text. More detailed energetic and structural results for the ground, and second- and third-most-stable cation binding modes calculated for each nucleoside are available in the Supplementary Material (Tables S2–S4, Figures S4–S5). Overall, highly parallel results are computed for the various nucleosides, with the most significant deviations occurring in the structures and energetics of the m^7Guo systems. In the ground neutral conformations, all nucleosides except m^7Guo favor a *syn* orientation of guanine[67,68] that is stabilized by an O5′H···N3 hydrogen bond. In contrast, an *anti* guanine orientation, stabilized by an O2′H···N3 hydrogen bond, is preferred by m^7Guo. The ground conformers of the protonated and sodium cationized forms of all of the nucleosides prefer an *anti* guanine orientation, stabilized by a non-canonical C8H···O5′ hydrogen bond.

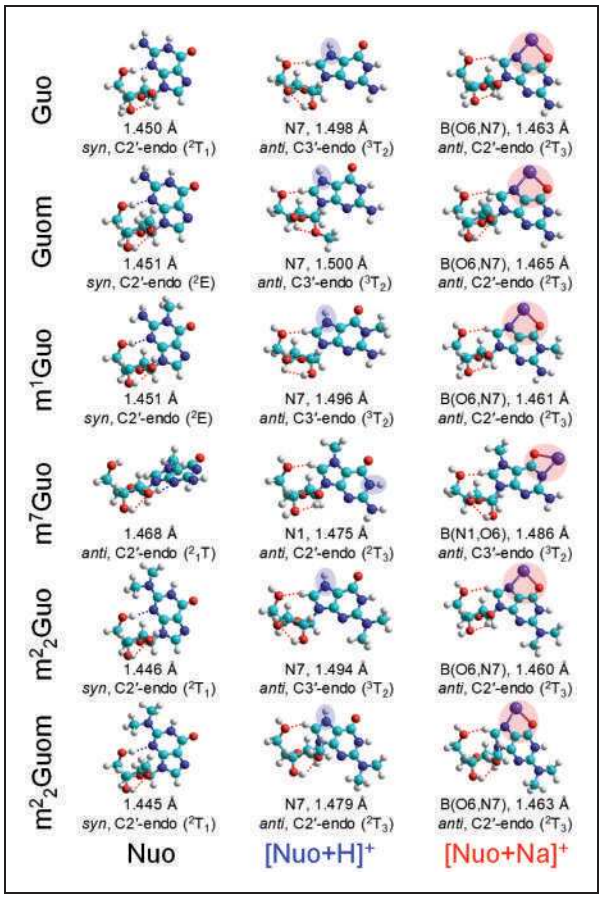

Figure 4. Calculated ground conformers of the neutral, protonated, and sodium cationized forms of guanosine and the methylguanosines. Protonation sites are highlighted in blue, and sodium cationization chelation rings are highlighted in red. The site of protonation or sodium cation binding, C1′–N9 glycosidic bond length, guanine orientation, and sugar puckering descriptions are given. Structures for Guo are taken from previous work.[52,64]

In all ground Nuo, $[Nuo+H]^+$, and $[Nuo+Na]^+$ conformers, either C2′-endo (also known as "South") or C3′-endo (also known as "North") sugar puckering[67,68] are favored. More specific sugar puckering designations based on pseudorotation phase angles[52–56,67,68] include $^2T_1$, $^2T_3$, and $^2{}_1T$ for the C2′-endo conformers, but only $^3T_2$ for the C3′-endo conformers. All ground neutrals, including m^7Guo, prefer C2′-endo ($^2T_1$, $^2T_3$, and $^2{}_1T$) sugar puckering. The ground $[Nuo+H]^+$ and $[Nuo+Na]^+$ sugar puckerings showcase the uniqueness of m^7Guo again. Both $[m^7Guo+H]^+$ and $[m^2{}_2Guom+H]^+$ adopt C2′-endo ($^2T_3$) sugar puckering, whereas the remaining $[Nuo+H]^+$ exhibit C3′-endo ($^3T_2$) sugar puckering. Similarly, $[m^7Guo+Na]^+$ adopts C3′-endo ($^3T_2$) sugar puckering, whereas all of the other $[Nuo+Na]^+$ complexes exhibit C2′-endo ($^2T_3$) sugar puckering. The ground neutrals exhibit the greatest variation in C2′-endo sugar puckering, including $^2T_1$, $^2T_3$, and $^2{}_1T$ designations, whereas the ground $[Nuo+H]^+$ and $[Nuo+Na]^+$ only display $^2T_3$ and $^3T_2$ designations in their C2′-endo and C3′-endo sugar puckerings, respectively.

Theoretical calculations: Cationization sites

The most favorable protonation site for all Nuo studied except m^7Guo (i.e. Guo, Guom m^1Guo, $m^2{}_2Guo$, and $m^2{}_2Guom$) is at the N7 position (0.0 kJ/mol). The next most stable protonation site of these nucleosides is at the O6 position (~35 kJ/mol), followed by the N3 position (~45 kJ/mol). The most favorable protonation site of m^7Guo is calculated to be the N1 position (0.0 kJ/mol), followed by O6 (16.8 kJ/mol) and N3 (61.0 kJ/mol). The calculations therefore predict O6-protonated $[m^7Guo+H]^+$ to be ~18 kJ/mol relatively more stable than predicted for the other nucleosides. The opposite trend is true for N3 protonation, where $[m^7Guo+H]^+$ is ~16 kJ/mol less stable than found for the other nucleosides.

The most stable binding modes for all $[Nuo+Na]^+$ studied here involve bidentate interactions between the

nucleobase and the sodium cation. In all nucleosides except m^7Guo the ground conformers involve binding interactions of the sodium cation with the O6 and N7 atoms of the nucleobase, designated B(O6,N7), creating a five-membered chelation ring. Because the N7 site is blocked by methylation in m^7Guo, the ground conformer involves bidentate interaction of the sodium cation with the N1 and O6 atoms of the nucleobase, designated B(N1,O6), creating a four-membered chelation ring. For all six nucleosides, the second most stable sodium cation binding modes involve tridentate interactions with the nucleobase and sugar heteroatoms, and are found ~60 kJ/mol above the corresponding ground conformers.

Discussion

Primary considerations for QIT MS ER-CID comparisons

$CID_{50\%}$ is an empirical value extracted from the survival yield analysis of ER-CID experiments. Survival yield curves are directly dependent on the mass spectrometer and experimental conditions used for their determination. When acquired under properly comparable conditions, survival yield analyses provide qualitative to semiquantitative measures of bond stabilities.[69–76] Survival yields depend on the collision gas pressure, electric field excitation intensity, excitation time window, ion energy distributions, ion size (i.e. number of degrees of freedom), reaction entropy, and the available reaction time. The collision gas pressure, auxiliary rf excitation amplitude, and excitation time window are readily controlled experimental parameters affecting the $CID_{50\%}$ value extracted. Ion energy distributions, sizes (Table S5), and reaction channels are important indirectly controlled experimental variables—these parameters are discussed to some degree in the Supplementary Material. To make valid comparisons of survival yield measurements across multiple nucleoside systems, the same collision gas pressures and excitation times must be applied during the rf excitation amplitude ramps, and experiments must be performed on systems with similar sizes and parallel reaction pathways to produce similar entropic effects.

Reaction products and mechanisms

N-glycosidic bond cleavage with retention of the cation by the nucleobase, the sole fragmentation channel observed in the reactions performed here, is often the intrinsically lowest energy unimolecular dissociation pathway observed in the CID of nucleosides (see the Supplementary Material for a more in-depth overview of the canonical nucleoside CID reaction products).[52–56,60–64] In previous work by Wu et al.,[61] the fragmentation pathways observed for gas phase $[Guo+H]^+$ and $[dGuo+H]^+$ were mechanistically mapped to proceed through a stepwise E1 elimination reaction by electronic structure calculations and comparisons with guided ion beam mass spectrometry (GIBMS) TCID activation energy thresholds. These results suggest the solvent-free substitution reaction pathway to proceed first by the rate-limiting elongation/cleavage of the C1′–N9 glycosidic bond, forming an oxocarbenium ion-like transition state on the sugar and an interaction of the N9 heteroatom electron density with the C2′H hydrogen, followed by transfer of that C2′ proton to the N9 atom of the nucleobase with the formation of a C1′=C2′ π-bond and an unsaturated planar sugar moiety. A parallel S_N1 reaction pathway involving water was separately mapped in a computational study as the lowest energy dissociation pathways for neutral and protonated m^7dGuo where it was found that protonation significantly reduced (by ~110–140 kJ/mol) the reaction activation energy.[77] The highly parallel sizes and structures of the reactants and fragments make it reasonable to expect parallel fragmentation processes to be undertaken by all of the nucleoside ions studied in this work. Therefore, entropic differences are assumed to be small enough to provide reliable trends in the relative bond activation energies measured via ER-CID.

Comparisons with canonical nucleoside stability measurements

Overall, the QIT MS ER-CID and GIBMS TCID reports on the canonical nucleosides consistently display two major trends: one, the RNA nucleoside glycosidic bonds are more stable than their DNA counterparts, and two, protonation activates the glycosidic bonds more effectively than sodium cationization.[52–56,60–63] For example, the RNA guanosine form, Guo, requires more energy to cleave its glycosidic bond than the DNA form, dGuo.[52,61] The TCID studies of $[Guo+H]^+$ and $[dGuo+H]^+$ yielded bond activation energies of 114.8 ± 2.9 and 93.6 ± 2.9 kJ/mol, respectively.[61] Thus, the 2′-deoxy modification of $[dGuo+H]^+$ weakens the glycosidic bond by ~21 kJ/mol versus $[Guo+H]^+$. QIT MS ER-CID results reaffirmed this trend with $CID_{50\%}$ values of 0.220 ± 0.002 V for $[Guo+H]^+$ and 0.186 ± 0.001 V for $[dGuo+H]^+$.[52]

All protonated methylguanosines studied here exhibit higher $CID_{50\%}$ values than $[dGuo+H]^+$, with $[m^1Guo+H]^+$ and $[Guom+H]^+$ less than $[Guo+H]^+$, $[m^7Guo+H]^+$ approximately equal to $[Guo+H]^+$, and $[m^2{}_2Guo+H]^+$ and $[m^2{}_2Guom+H]^+$ greater than $[Guo+H]^+$ but less than $[dAdo+H]^+$ (0.252 ± 0.001 V).[53] Of the sodium cationized methylguanosines studied here, only $[m^7Guo+Na]^+$ requires lower activation energy than $[dGuo+Na]^+$ (0.260 ± 0.002 V), and the remaining values are greater than for $[Guo+Na]^+$ but less than found for $[dAdo+Na]^+$ (0.378 ± 0.004 V).[53] Further GIBMS TCID measurements on $[Guo+Na]^+$, $[dGuo+Na]^+$,

and the methylguanosines are expected to mimic the gross trends in the ER-CID data acquired in this work, while further solidifying the mechanistic details and quantitative energetics of their glycosidic bond cleavage processes.

$CID_{50\%}$ and other dissociation levels

The survival yield curves for all of the $[Nuo+Na]^+$ complexes are highly parallel (see Figure 2 and Figure S3), and therefore, relative stability assessments are robust and unaffected by the choice of arbitrary dissociation level used. Unfortunately, this is not the case for the $[Nuo+H]^+$ survival yield curves. The primary outlier is $[Guom+H]^+$, as its dissociation onset begins between that of $[m^2{}_2Guom+H]^+$ and $[m^2{}_2Guo+H]^+$, making it appear as the second most stable protonated species. However, its $CID_{50\%}$ value lies between that of $[m^1Guo+H]^+$ and $[Guo+H]^+$ or $[m^7Guo+H]^+$, and near the end of the dissociation curve it appears less stable than $[m^1Guo+H]^+$, the least stable nucleoside examined here. The $[m^2{}_2Guo+H]^+$ and $[m^2{}_2Guom+H]^+$ curves both fall below that of $[Guo+H]^+$ with survival yields less than ~0.15. The accuracy of these particular stability assessments is therefore somewhat questionable, but their values certainly all lie within the regime of the other $[Nuo+H]^+$.

Calculated glycosidic bond lengths versus experimental $CID_{50\%}$

Depending on the reaction coordinate specifics, equilibrium bond lengths may display a linear relationship with the free energy of activation for its heterolytic cleavage.[78–80] A reasonably linear correlation (R^2 = 0.8016) between the $CID_{50\%}$ values and the calculated C1′–N9 glycosidic bond lengths of the ground conformers predicted in this work is found as shown in Figure 5. In general, less activation energy is required for dissociation with increasing equilibrium *N*-glycosidic bond length of the ground conformers. $[m^7Guo+H]^+$ deviates the furthest from the linear correlation. These results also support parallel methylguanosine reaction coordinates with those mapped for $[Guo+H]^+$ and $[dGuo+H]^+$ in previous work,[61] where the rate-limiting step for unimolecular dissociation begins with elongation of the *N*-glycosidic bond.

Effects of cationization and methylation on glycosidic bond lengths and $CID_{50\%}$

The neutral forms of the nucleosides have on average the shortest calculated C1′–N9 glycosidic bond lengths (1.452 Å, normalized to 0.000 Å), followed by the sodium cationized forms (1.466 Å, ~0.018 Å longer), and finally by the protonated forms (1.490 Å, ~0.038 Å longer) (see Figure 4), suggesting the relative reactivities to generally increase from neutral < sodium cationized < protonated. This is

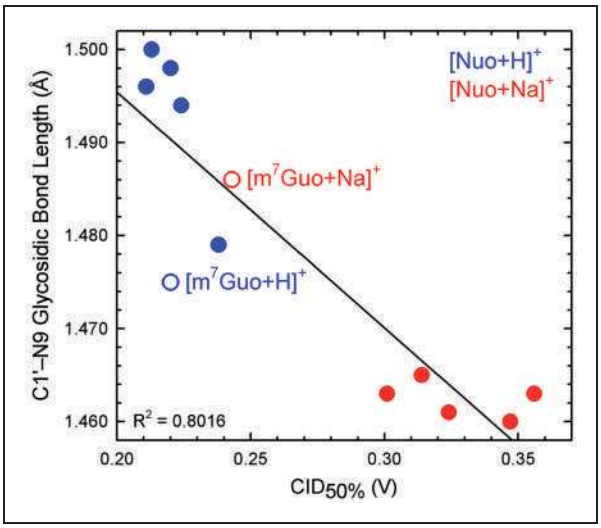

Figure 5. Experimental $CID_{50\%}$ values plotted against the calculated *N*-glycosidic bond lengths of the ground conformers of the protonated (blue) and sodium cationized (red) forms of guanosine and the methylguanosine nucleosides shown in Figure 4. The m^7Guo data points are labeled and indicated with open circles. The black line represents the linear regression best fit line through all of the data. Error bars for the $CID_{50\%}$ values are approximately half the diameter of the symbols as shown.

supported by the experimental results, as all $[Nuo+H]^+$ exhibit lower $CID_{50\%}$ values than the $[Nuo+Na]^+$. The two $[Nuo+H]^+$ with C2′-endo ground sugar puckering, $[m^7Guo+H]^+$ and $[m^2{}_2Guom+H]^+$, are the only two $[Nuo+H]^+$ with C1′–N9 bond lengths shorter than $[m^7Guo+Na]^+$, which was the only $[Nuo+Na]^+$ complex with C2′-endo ground sugar puckering. Overall, the experimental results, especially for the sodium cationized conformers, generally show that increased nucleoside stability comes with increasing methyl substitution (canonical < mono- < di- < trimethylated). Exceptions include $[m^1Guo+H]^+$ and $[Guom+H]^+$, with lower $CID_{50\%}$ values than $[Guo+H]^+$.

The simple analysis of electronegativity and electron-donating character of the described modifications is often useful in understanding molecular trends. The electron deficiency of the N7–$CH_3{}^+$ substituent of m^7Guo produces electron-withdrawing character that pulls electron density out of the purine ring system, lengthens and activates the C1′–N9 glycosidic bond, and reduces the energy required for the unimolecular dissociation reaction. The glycosidic bond lengths predicted increase by 0.018 Å from Guo to m^7Guo, by 0.007 Å from m^7Guo to $[m^7Guo+H]^+$, and by 0.018 Å from m^7Guo to $[m^7Guo+Na]^+$. Based solely on their ground glycosidic bond lengths, $[m^7Guo+H]^+$ would be expected to exhibit a lower activation energy than $[m^7Guo+Na]^+$, in contrast to that experimentally observed. $[m^7Guo+H]^+$ exhibits a $CID_{50\%}$ value 0.023 V lower than $[m^7Guo+Na]^+$, indicating protonation is still slightly more activating than

sodium cationization. The $CID_{50\%}$ value for $[m^7Guo+Na]^+$ is ~0.085 V lower than the average $CID_{50\%}$ for the other sodium cationized nucleosides. Overall, the combined relative $CID_{50\%}$ values and C1′–N9 lengths suggest N7-methylation to be more activating than the subsequent cationization.

The various nucleobase methylations of m^1Guo, $m^2{}_2Guo$, and $m^2{}_2Guom$ are expected to donate electron density into the π-cloud of the aromatic purine nucleobases, increasing the substitution reaction barrier by stabilizing the glycosidic bond and making the nucleobase a worse leaving group. However, minimal glycosidic bond shortening is predicted for these neutral nucleosides. The largest and second largest bond length decreases relative to Guo are predicted for $m^2{}_2Guom$ (0.005 Å) and $m^2{}_2Guo$ (0.004 Å), correlating well with their relative stabilities ($m^2{}_2Guom > m^2{}_2Guo$). In contrast, the m^1Guo glycosidic bond lengthened by 0.001 Å. This bond lengthening is consistent with the lower $CID_{50\%}$ of $[m^1Guo+H]^+$ compared with $[Guo+H]^+$, but inconsistent with the higher $CID_{50\%}$ of $[m^1Guo+Na]^+$ with $[Guo+Na]^+$.

The effects of O2′-methylation and the resulting C2′-methoxy groups of Guom and $m^2{}_2Guom$ are the most difficult to establish clear trends for. Electronegativity and inductive electronic effects of the 2′-substituents can produce permanent bond dipoles affecting the 2′-carbon of the sugar. Partial positive character at the C2′-position electrostatically clashes with the partial positive character of the oxocarbenium intermediate, destabilizing the reaction intermediate and driving up the reaction energy requirements. Partial negative character at this position would generally produce the opposite effect, stabilizing the reaction intermediate and reducing the energy requirements. Based solely on electronegativity,[81] the less electronegative methoxy groups of Guom and $m^2{}_2Guom$ would be less destabilizing to the rate-limiting transition states than the hydroxyl substituents of the canonical ribose sugars, and thus their apparent glycosidic bond strengths are expected to be lower. Additionally, methoxy substituents are expected to be more inductively electron donating than hydroxy groups, again suggesting lower activation energy requirements. This assessment can potentially explain the lower $CID_{50\%}$ of $[Guom+H]^+$ relative to $[Guo+H]^+$, but does not explain the higher $CID_{50\%}$ of $[Guom+Na]^+$ relative to $[Guo+Na]^+$.

Cation binding sites of the calculated conformers

Protonation of Guo (and dGuo) via ESI has been previously confirmed via IRMPD action spectroscopy to dominantly occur at the N7 position (as shown in Figure 4, second column), followed by the O6 and then N3 positions.[64] Single point energy calculations performed in that work (and used for comparisons here) at the B3LYP/6-311+G(2d,2p) level of theory using the B3LYP/6-311+G(d,p) optimized structures predicted the relative Gibbs free energy of the lowest energy conformer for each $[Guo+H]^+$ protonation site to be 0.0 kJ/mol for N7, 35.0 kJ/mol for O6, and 41.2 kJ/mol for N3.[64] The calculations performed here predict the same relative trends for all of the guanosine derivatives studied here except $[m^7Guo+H]^+$ (see Figure 4, Figures S5–S6, and Tables S2–S4), providing additional evidence that the trends reported here are reliable, but confirmation via future IRMPD experiments is desirable. Previous solid- and solution-phase studies of m^7Guo have also shown preferential protonation at the N1 position.[82,83] The ground N1 protonation position of $[m^7Guo+H]^+$ makes sense as the proton can form a strong covalent bond with the N1 atom of the m^7Guo zwitterion, forming the traditional m^7Guo structure with an intrinsically positively charged $N7–CH_3{}^+$ methyl cation. Whereas $[m^7Guo+H]^+$ is more properly characterized as a "methyl cationized" nucleoside, all other cationic $[Nuo+H]^+$ are better described as traditional "protonated" nucleosides.

The sodium cation binding modes of Guo (and dGuo) produced in ESI have been confirmed via IRMPD action spectroscopy to solely involve a bidentate charge-solvated interaction of the Na^+ with the O6 and N7 atoms of the nucleobase forming a five-membered chelation ring (as shown in Figure 4, third column).[53] The results for the modified guanosines are highly parallel to those predicted for $[Guo+Na]^+$ and $[dGuo+Na]^+$ in all cases except for $[m^7Guo+Na]^+$, as expected. In $[m^7Guo+Na]^+$, bidentate (N1,O6) sodium cation binding is stabilized by shielding the partial negative character of the m^7Guo zwitterion through the formation of a $Na^+\cdots O6^-\cdots C7H_3{}^+$ salt-bridge structure similar to those observed in metal cationized amino acids.[84–91]

Guanine orientation and sugar puckering of the calculated conformers

An *anti* orientation of guanine is predicted to be favored over a *syn* orientation in the ground structures of all $[Nuo+H]^+$ and $[Nuo+Na]^+$ examined here. These results are consistent with previous complementary IRMPD and theoretical studies of $[Guo+H]^+$, $[dGuo+H]^+$, $[Guo+Na]^+$, and $[dGuo+Na]^+$,[52,64] as well as solid- and solution-phase studies of Guo and dGuo,[92,93] as an *anti* nucleobase orientation is preferred in all cases. Upon cocrystallization, m^7Guo had *syn* orientation while the $[m^7Guo+H]^+$ had *anti* orientation.[83] In solution, m^7Guo preferred *syn* orientation, while $[m^7Guo+H]^+$ had a mixture of *syn* and *anti* orientations.[82] The *anti* orientation facilitates Watson–Crick base pairing of canonical nucleosides in vivo. However, the methyl modifications studied here would generally unfavorably impact canonical base pairing via removal of hydrogen bond donors and acceptors. When Guo or dGuo pairs with cytidine (Cyd) or 2′-deoxycytidine (dCyd), the O6 position of guanine acts as a hydrogen

Table 2. Theoretical nucleoside proton affinities at 0 and 298 K, and gas-phase basicities at 298 K.[a]

Nucleoside	Protonation Site	PA_0	Relative PA_0	PA_{298}	Relative PA_{298}	GB_{298}	Relative GB_{298}
Guo	N7	975.5	0.0	980.2	0.0	951.6	0.0
Guom	N7	983.6	8.1	987.2	7.0	960.9	9.2
m^1Guo	N7	991.9	16.4	996.1	15.9	968.6	16.9
m^7Guo	N1	1054.2	78.7	1058.1	77.9	1027.3	75.7
$m^2{}_2$Guo	N7	1006.1	30.6	1011.1	30.9	982.6	31.0
$m^2{}_2$Guom	N7	1004.0	28.6	1008.2	28.0	982.9	31.3

[a]All values are reported in kJ/mol. Relative values given with respect to Guo. Geometry optimizations and frequency analyses were performed at the B3LYP/6-311+G(d,p) level of theory with a frequency scaling factor of 0.9887.[66] Single point energies were calculated at the B3LYP/6-311+G(2d,2p) level of theory. All calculations were performed at standard ambient temperature and pressure.

bond acceptor, while the N1 and N2 positions of guanine act as hydrogen bond donors. Methylations at the N1 (as in m^1Guo) and N2 positions (as in $m^2{}_2$Guo and $m^2{}_2$Guom) would clearly disrupt these Watson–Crick edge interactions. The gas-phase neutral forms of nearly all Nuo studied except m^7Guo are predicted to favor a *syn* orientation, suggesting both cationization and solvation induce nucleobase rotation. Interestingly, m^7Guo again differs from the other nucleosides as its ground neutral form prefers an *anti* orientation of guanine.

Only C2′-endo (South) and C3′-endo (North) sugar puckerings are predicted for the ground neutral, protonated, and sodium cationized nucleosides. These sugar puckerings are the most common forms naturally adopted by nucleic acids, with RNA generally adopting C3′-endo and DNA generally adopting C2′-endo. The calculations in this work generally suggest the neutral and sodium cationized forms to prefer C2′-endo sugar puckering, whereas the protonated forms prefer C3′-endo sugar puckering. In the O2′-methylated nucleosides (Guom and $m^2{}_2$Guom) the O2′ substituent is unable to act as a hydrogen bond donor, limiting the available intramolecular stabilizing interactions, although this did not have a major effect on the preferred sugar puckerings.

Theoretical proton affinities

With the calculation of the ground neutral and protonated forms of each nucleoside, theoretical PAs and gas-phase basicities (GBs) for each protonation site can be calculated as the negative of the enthalpy change ($-\Delta H_{rxn}$) and the negative of the Gibbs free energy change ($-\Delta G_{rxn}$), respectively, for reaction (4)

$$Nuo+H^+ \rightarrow [Nuo+H]^+ \quad (4)$$

The PA value at 298 K (PA_{298}) for the most favorable protonation site corresponds to the thermodynamic PA of the nucleoside (see Table 2). The discussion in this section primarily regards the PA_{298}, but PA values at 0 K (PA_0) and GB values at 298 K (GB_{298}) are included in Table 2 for completeness and for reference. The PAs and GBs for the less favorable protonation sites can be calculated (see Table S6), but are useful in limited situations. The trends in PA_0 and GB_{298} generally mimic the trends in PA_{298}, with PA_{298} being ~4 kJ/mol greater than PA_0, and PA_{298} being ~28 kJ/mol greater than GB_{298}.

Previous experimental and theoretical results generally indicate guanine to have the highest PA of the canonical nucleobases.[94–99] All methylations studied here increase the theoretical PA. The m^7Guo zwitterion exhibits the highest PA among the nucleosides examined here, where accepting a proton neutralizes the negative charge of the zwitterion, forming a stable formally cationic structure. In m^1Guo, the electron-donating characteristics of its single guanine methylation increase the PA_{298} by 15.9 kJ/mol. The increase in PA_{298} for $m^2{}_2$Guo and $m^2{}_2$Guom is nearly double (30.9 and 28.0 kJ/mol, respectively) in response to doubling the guanine methyl substituents and the corresponding increase in electron donation into the aromatic purine ring system. However, the methylation positions changed between the singly and doubly methylated nucleosides, so other effects such as proximity preclude direct comparisons. Interestingly, O2′-methylation increases the PA by 7.0 kJ/mol from Guo to Guom, but decreases the PA_{298} by 2.9 kJ/mol from $m^2{}_2$Guo to $m^2{}_2$Guom. These somewhat conflicting effects of O2′-methylation are also apparent in the relative glycosidic bond stabilities, where the $CID_{50\%}$ value decreases from $[Guo+H]^+$ to $[Guom+H]^+$, but increases from $[Guo+Na]^+$ to $[Guom+Na]^+$.

Conclusions

Protonation is known to activate nucleoside *N*-glycosidic bonds in solution and in biological enzyme-catalyzed nucleobase-excision reactions. Beyond sterically affecting enzyme–substrate interactions, methylations intrinsically influence the activation barriers for *N*-glycosidic bond cleavages, as evidenced by the QIT MS ER-CID experimental results. The C1′–N9 glycosidic bond lengths from DFT calculations support and complement the experiments. As expected, the protonated forms of the five

naturally occurring methylguanosines studied, Guom, m^1Guo, m^7Guo, $m^2{}_2$Guo, and $m^2{}_2$Guom, require less activation energy for intramolecular *N*-glycosidic bond cleavage than their sodium cationized counterparts. The activation energy required for m^7Guo fragmentation is similar whether protonated or sodium cationized, and similar to that of the other protonated methylguanosines. Perhaps most interestingly, experimental and theoretical results suggest that N7-methylation is intrinsically more activating than protonation or sodium cationization. The $CID_{50\%}$ values suggest that the relative nucleoside *N*-glycosidic bond strengths roughly increase in the order $m^1Guo < Guom < Guo < m^7Guo < m^2{}_2Guo, < m^2{}_2Guom$ when protonated, and in the order $m^7Guo << Guo < Guom < m^1Guo < m^2{}_2Guo < m^2{}_2Guom$ when sodium cationized. The di- and trimethylated guanosines, $m^2{}_2$Guo and $m^2{}_2$Guom, exhibit the most stable glycosidic bonds, supporting their role as thermally stable modifications found in extreme thermophiles. All methylated derivatives increase the theoretical proton affinities compared with canonical Guo. Compared to the other methylguanosines, N7-methylation alters the preferred site of protonation from the N7 to the N1 atom, and the Na^+ binding site from a bidentate (O6,N7) charge-solvated interaction to a bidentate (N1,O6) interaction, forming a $Na^+\cdots O6^-\cdots C7H_3{}^+$ salt-bridge structure.

Follow-up GIBMS TCID experiments for all of these nucleoside complexes are ultimately desirable as they would provide quantitative intrinsic activation energies by explicitly accounting for the reaction frequency factors and analytically reducing the CID experiments to single collisions. These experiments would further validate the QIT MS ER-CID trends and quantitatively assess the activation energies required for the intrinsic (solvent-free) *N*-glycosidic bond cleavages. IRMPD action spectroscopy is also of interest to firmly establish the gas-phase structural conformations. Condensed-phase and in vivo studies involving sodium cation-mediated activation of m^7Guo could also be of interest. Overall, there is still much to learn and tease apart in the world of nucleic acids.

Acknowledgements

The authors thank Wayne State University (WSU) Computing and Information Technology (C&IT) for computational resources and support. The authors gratefully acknowledge Lucas Hamlow (WSU) for developing useful data analysis software. The authors acknowledge Chenchen He (WSU) for performing initial $[Guom+H]^+$ calculations. The authors thank Christine S. Chow (WSU) for her thoughts and suggestions during manuscript preparation. The authors are exceedingly appreciative of James A. McCloskey and Patrick A. Limbach for providing us with the m^1Guo, m^7Guo, $m^2{}_2$Guo, and $m^2{}_2$Guom samples. These samples were extracted from natural sources by J. A. McCloskey and P. A. Limbach at the Departments of Medicinal Chemistry and Biochemistry, University of Utah (Salt Lake City, UT, USA). The samples were then taken to the University of Cincinnati (Cincinnati, OH, USA) under the care of P. A. Limbach, where they were eventually provided to M. T. Rodgers for studies at WSU.

Declaration of conflicting interests

The author(s) declared no potential conflicts of interest with respect to the research, authorship, and/or publication of this article.

Funding

The author(s) disclosed receipt of the following financial support for the research, authorship, and/or publication of this article: This work was supported by the National Science Foundation grant numbers DBI-0922819, for the Bruker amaZon ETD QIT MS, and CHE-1709789, for all other research costs. ZJD and YZ gratefully acknowledge support from Wayne State University Thomas C. Rumble Graduate Fellowships, and ZJD is thankful for additional support from the Joseph Jasper Scholarship for Graduate Students in Chemistry.

ORCID iDs

Zachary J Devereaux http://orcid.org/0000-0002-8385-3492
MT Rodgers http://orcid.org/0000-0002-5614-0948

References

1. Moore MJ. From birth to death: the complex lives of eukaryotic mRNAs. *Science* 2005; 309: 1514–1518.
2. Decatur WA and Fournier MJ. RNA-guided nucleotide modification of ribosomal and other RNAs. *J Biol Chem* 2003; 278: 695–698.
3. Maas S and Rich A. Changing genetic information through RNA editing. *BioEssays* 2000; 22: 790–802.
4. Jackman JE and Alfonzo JD. Transfer RNA modifications: nature's combinatorial chemistry playground. *Wiley Interdiscip Rev RNA* 2013; 4: 35–48.
5. Lorenz C, Lünse C and Mörl M. tRNA modifications: impact on structure and thermal adaptation. *Biomolecules* 2017; 7: 35.
6. Omer AD, Ziesche S, Decatur WA, et al. RNA-modifying machines in archaea. *Mol Microbiol* 2003; 48: 617–629.
7. Decatur WA and Fournier MJ. rRNA modifications and ribosome function. *Trends Biochem Sci* 2002; 27: 344–351.
8. Maden B. The numerous modified nucleotides in eukaryotic ribosomal RNA. In: Cohn W and Moldave K (eds) *Progress in nucleic acid research and molecular biology*, Amsterdam, The Netherlands: Elsevier, 1990, pp.241–303.
9. Wilson DN and Nierhaus KH. The weird and wonderful world of bacterial ribosome regulation. *Crit Rev Biochem Mol Biol* 2007; 42: 187–219.
10. Tran E, Brown J and Maxwell ES. Evolutionary origins of the RNA-guided nucleotide-modification complexes: from the primitive translation apparatus? *Trends Biochem Sci* 2004; 29: 343–350.
11. Isaksson LA and Phillips JH. Studies on microbial RNA: V. A comparison of the in vivo methylated components of ribosomal RNA from *Escherichia coli* and

Saccharomyces cerevisiae. *Biochim Biophys Acta* 1968; 155: 63–71.
12. Motorin Y and Helm M. RNA nucleotide methylation. *Wiley Interdiscip Rev RNA* 2011; 2: 611–631.
13. Boccaletto P, Machnicka MA, Purta E, et al. MODOMICS: a database of RNA modification pathways. *2017 update*. Nucleic Acids Res 2017; 46: D303–D307.
14. Cantara WA, Crain PF, Rozenski J, et al. The RNA modification database, RNAMDB: 2011 update. *Nucleic Acids Res* 2011; 39: D195–D201.
15. Limbach PA, Crain PF and McCloskey JA. Summary: the modified nucleosides of RNA. *Nucleic Acids Res* 1994; 22: 2183–2196.
16. Paul Agris PFC, Rozenski J, Fabris D, et al. *The RNA modification database*. New York: The RNA Institute, University at Albany, State University of New York, 2018.
17. Brimacombe R, Mitchell P, Osswald M, et al. Clustering of modified nucleotides at the functional center of bacterial ribosomal RNA. *FASEB J* 1993; 7: 161–167.
18. Bügl H, Fauman EB, Staker BL, et al. RNA methylation under heat shock control. *Mol Cell* 2000; 6: 349–360.
19. Noon KR, Bruenger E and McCloskey JA. Posttranscriptional modifications in 16S and 23S rRNAs of the archaeal hyperthermophile *Sulfolobus solfataricus*. *J Bacteriol* 1998; 180: 2883–2888.
20. Edmonds C, Crain P, Gupta R, et al. Posttranscriptional modification of tRNA in thermophilic archaea (archaebacteria). *J Bacteriol* 1991; 173: 3138–3148.
21. Edmonds CG, Crain PF, Hashizume T, et al. Structural characterization of four ribose-methylated nucleosides from the transfer RNA of extremely thermophilic archaebacteria. *J Chem Soc Chem Commun* 1987; 12: 909–910.
22. Kumagai I, Watanabe K and Oshima T. Thermally induced biosynthesis of 2′-O-methylguanosine in tRNA from an extreme thermophile, *Thermus thermophilus* HB27. *Proc Natl Acad Sci USA* 1980; 77: 1922–1926.
23. Kowalak JA, Dalluge JJ, McCloskey JA, et al. The role of posttranscriptional modification in stabilization of transfer RNA from hyperthermophiles. *Biochemistry* 1994; 33: 7869–7876.
24. Shen L, Song C-X, He C, et al. Mechanism and function of oxidative reversal of DNA and RNA methylation. *Annu Rev Biochem* 2014; 83: 585–614.
25. Fu Y, Dominissini D, Rechavi G, et al. Gene expression regulation mediated through reversible m6A RNA methylation. *Nat Rev Genet* 2014; 15: 293–306.
26. Fustin J-M, Doi M, Yamaguchi Y, et al. RNA-methylation-dependent RNA processing controls the speed of the circadian clock. *Cell* 2013; 155: 793–806.
27. Maden BEH. Locations of methyl groups in 28S rRNA of *Xenopus Laevis* and man: clustering in the conserved core of molecule. *J Mol Biol* 1988; 201: 289–314.
28. Kiss-László Z, Henry Y, Bachellerie J-P, et al. Site-specific ribose methylation of preribosomal RNA: a novel function for small nucleolar RNAs. *Cell* 1996; 85: 1077–1088.
29. Daffis S, Szretter KJ, Schriewer J, et al. 2′-O methylation of the viral mRNA cap evades host restriction by IFIT family members. *Nature* 2010; 468: 452.
30. Bjork G, Wikstrom P and Bystrom A. Prevention of translational frameshifting by the modified nucleoside 1-methylguanosine. *Science* 1989; 244: 986–989.
31. Urbonavičius J, Qian Q, Durand JM, et al. Improvement of reading frame maintenance is a common function for several tRNA modifications. *EMBO J* 2001; 20: 4863–4873.
32. Jackman JE, Montange RK, Malik HS, et al. Identification of the yeast gene encoding the tRNA m1G methyltransferase responsible for modification at position 9. *RNA* 2003; 9: 574–585.
33. Shatkin AJ. Capping of eucaryotic mRNAs. *Cell* 1976; 9: 645–653.
34. Wei CM and Moss B. Methylated nucleotides block 5′-terminus of vaccinia virus messenger RNA. *Proc Natl Acad Sci USA* 1975; 72: 318–322.
35. Muthukrishnan S, Both GW, Furuichi Y, et al. 5′-terminal 7-methylguanosine in eukaryotic mRNA is required for translation. *Nature* 1975; 255: 33.
36. Fechter P and Brownlee GG. Recognition of mRNA cap structures by viral and cellular proteins. *J Gen Virol* 2005; 86: 1239–1249.
37. Phizicky EM and Hopper AK. tRNA biology charges to the front. *Genes Dev* 2010; 24: 1832–1860.
38. Ellis SR, Morales MJ, Li J-M, et al. Isolation and characterization of the TRM1 locus, a gene essential for the N2,N2-dimethylguanosine modification of both mitochondrial and cytoplasmic tRNA in *Saccharomyces cerevisiae*. *J Biol Chem* 1986; 261: 9703–9709.
39. Ellis S, Hopper A and Martin N. Amino-terminal extension generated from an upstream AUG codon increases the efficiency of mitochondrial import of yeast N2,N2-dimethylguanosine-specific tRNA methyltransferases. *Mol Cell Biol* 1989; 9: 1611–1620.
40. Steinberg S and Cedergren R. A correlation between N2-dimethylguanosine presence and alternate tRNA conformers. *RNA* 1995; 1: 886–891.
41. Drabløs F, Feyzi E, Aas PA, et al. Alkylation damage in DNA and RNA – repair mechanisms and medical significance. *DNA Repair* 2004; 3: 1389–1407.
42. Falnes PØ, Klungland A and Alseth I. Repair of methyl lesions in DNA and RNA by oxidative demethylation. *Neuroscience* 2007; 145: 1222–1232.
43. Vohhodina J, Harkin DP and Savage KI. Dual roles of DNA repair enzymes in RNA biology/post-transcriptional control. *Wiley Interdiscip Rev RNA* 2016; 7: 604–619.
44. Berti PJ and McCann JAB. Toward a detailed understanding of base excision repair enzymes: transition state and mechanistic analyses of N-glycoside hydrolysis and N-glycoside transfer. *Chem Rev* 2006; 106: 506–555.
45. O'Brie PJ and Ellenberger T. Human alkyladenine DNA glycosylase uses acid−base catalysis for selective excision of damaged purines. *Biochemistry* 2003; 42: 12418–12429.
46. Rodgers M, Campbell S, Marzluff EM, et al. Site-specific protonation directs low-energy dissociation pathways of dinucleotides in the gas phase. *Int J Mass Spectrom Ion Process* 1995; 148: 1–23.
47. McCann JA and Berti PJ. Transition state analysis of acid-catalyzed dAMP hydrolysis. *J Am Chem Soc* 2007; 129: 7055–7064.
48. Drohat AC and Maiti A. Mechanisms for enzymatic cleavage of the N-glycosidic bond in DNA. *Org Biomol Chem* 2014; 12: 8367–8378.

49. Zoltewicz JA, Clark DF, Sharpless TW, et al. Kinetics and mechanism of the acid-catalyzed hydrolysis of some purine nucleosides. *J Am Chem Soc* 1970; 92: 1741–1750.
50. Memboeuf A, Jullien L, Lartia R, et al. Tandem mass spectrometric analysis of a mixture of isobars using the survival yield technique. *J Am Soc Mass Spectrom* 2011; 22: 1744.
51. Green-Church KB and Limbach PA. Mononucleotide gas-phase proton affinities as determined by the kinetic method. *J Am Soc Mass Spectrom* 2000; 11: 24–32.
52. Zhu Y, Hamlow LA, He CC, et al. Gas-phase conformations and N-glycosidic bond stabilities of sodium cationized 2′-deoxyguanosine and guanosine: sodium cations preferentially bind to the guanine residue. *J Phys Chem B* 2017; 121: 4048–4060.
53. Zhu Y, Hamlow LA, He CC, et al. Influence of sodium cationization versus protonation on the gas-phase conformations and glycosidic bond stabilities of 2′-deoxyadenosine and adenosine. *J Phys Chem B* 2016; 120: 8892–8904.
54. Zhu Y, Roy HA, Cunningham NA, et al. IRMPD action spectroscopy, ER-CID experiments, and theoretical studies of sodium cationized thymidine and 5-methyluridine: kinetic trapping during the ESI desolvation process preserves the solution structure of $[Thd+Na]^+$. *J Am Soc Mass Spectrom* 2017; 28: 2423–2437.
55. Zhu Y, Roy HA, Cunningham NA, et al. Effects of sodium cationization versus protonation on the conformations and N-glycosidic bond stabilities of sodium cationized Urd and dUrd: solution conformation of $[Urd+Na]^+$ is preserved upon ESI. *Phys Chem Chem Phys* 2017; 19: 17637–17652.
56. Zhu Y, Hamlow LA, He CC, et al. Conformations and N-glycosidic bond stabilities of sodium cationized 2′-deoxycytidine and cytidine: solution conformation of $[Cyd+Na]^+$ is preserved upon ESI. *Int J Mass Spectrom* 2017; 429: 18–27.
57. Zhu Y, Yang Z and Rodgers MT. Influence of linkage stereochemistry and protecting groups on glycosidic bond stability of sodium cationized glycosyl phosphates. *J Am Soc Mass Spectrom* 2017; 28: 2602–2613.
58. Azargun M and Fridgen TD. Guanine tetrads: an IRMPD spectroscopy, energy resolved SORI-CID, and computational study of $M(9\text{-Ethylguanine})_4^+$ ($M = Li$, Na, K, Rb, Cs) in the gas phase. *Phys Chem Chem Phys* 2015; 17: 25778–25785.
59. Rosu F, Pirotte S, Pauw ED, et al. Positive and negative ion mode ESI-MS and MS/MS for studying drug–DNA complexes. *Int J Mass Spectrom* 2006; 253: 156–171.
60. Wu RR and Rodgers MT. Mechanisms and energetics for N-glycosidic bond cleavage of protonated adenine nucleosides: N3 protonation induces base rotation and enhances N-glycosidic bond stability. *Phys Chem Chem Phys* 2016; 18: 16021–16032.
61. Wu RR, Chen Y and Rodgers MT. Mechanisms and energetics for N-glycosidic bond cleavage of protonated 2′-deoxyguanosine and guanosine. *Phys Chem Chem Phys* 2016; 18: 2968–2980.
62. Wu RR and Rodgers MT. O2 protonation controls threshold behavior for N-glycosidic bond cleavage of protonated cytosine nucleosides. *J Phys Chem B* 2016; 120: 4803–4811.
63. Wu RR and Rodgers MT. Tautomerization lowers the activation barriers for N-glycosidic bond cleavage of protonated uridine and 2′-deoxyuridine. *Phys Chem Chem Phys* 2016; 18: 24451–24459.
64. Wu RR, Yang B, Berden G, et al. Gas-phase conformations and energetics of protonated 2′-deoxyguanosine and guanosine: IRMPD action spectroscopy and theoretical studies. *J Phys Chem B* 2014; 118: 14774–14784.
65. Frisch MJ, Trucks GW, Schlegel HB, et al. *Gaussian 09*. Wallingford, CT: Gaussian, Inc., 2009.
66. Merrick JP, Moran D and Radom L. An evaluation of harmonic vibrational frequency scale factors. *J Phys Chem A* 2007; 111: 11683–11700.
67. Altona C and Sundaralingam M. Conformational analysis of the sugar ring in nucleosides and nucleotides. Improved method for the interpretation of proton magnetic resonance coupling constants. *J Am Chem Soc* 1973; 95: 2333–2344.
68. Altona C and Sundaralingam M. Conformational analysis of the sugar ring in nucleosides and nucleotides. New description using the concept of pseudorotation. *J Am Chem Soc* 1972; 94: 8205–8212.
69. Bazsó FL, Ozohanics O, Schlosser G, et al. Quantitative comparison of tandem mass spectra obtained on various instruments. *J Am Soc Mass Spectrom* 2016; 27: 1357–1365.
70. Memboeuf A, Nasioudis A, Indelicato S, et al. Size effect on fragmentation in tandem mass spectrometry. *Anal Chem* 2010; 82: 2294–2302.
71. KukiÁ, Nagy L, Memboeuf A, et al. Energy-dependent collision-induced dissociation of Lithiated polytetrahydrofuran: effect of the size on the fragmentation properties. *J Am Soc Mass Spectrom* 2010; 21: 1753–1761.
72. Kertesz TM, Hall LH, Hill DW, et al. CE50: quantifying collision-induced dissociation energy for small molecule characterization and identification. *J Am Soc Mass Spectrom* 2009; 20: 1759–1767.
73. Guo X, Duursma MC, Kistemaker PG, et al. Manipulating internal energy of protonated biomolecules in electrospray ionization Fourier transform ion cyclotron resonance mass spectrometry. *J Mass Spectrom* 2003; 38: 597–606.
74. Vékey K. Internal energy effects in mass spectrometry. *J Mass Spectrom* 1996; 31: 445–463.
75. Hart KJ and McLuckey SA. Relative dissociation energy measurements using ion trap collisional activation. *J Am Soc Mass Spectrom* 1994; 5: 250–259.
76. Derwa F, De Pauw E and Natalis P. New basis for a method for the estimation of seconary ion internal energy distribution in 'soft' ionization techniques. *J Mass Spectrom* 1991; 26: 117–118.
77. Rios-Font R, Rodríguez-Santiago L, Bertran J, et al. Influence of N7 protonation on the mechanism of the N-glycosidic bond hydrolysis in 2′-deoxyguanosine. A theoretical study. *J Phys Chem B* 2007; 111: 6071–6077.
78. Jones PG and Kirby AJ. Simple correlation between bond length and reactivity. Combined use of crystallographic and kinetic data to explore a reaction coordinate. *J Am Chem Soc* 1984; 106: 6207–6212.
79. Allen FH and Kirby AJ. Bond length and reactivity. Variable length of the carbon-oxygen single bond. *J Am Chem Soc* 1984; 106: 6197–6200.

80. Jones PG and Kirby AJ. Linear relationship between bond length and reactivity. *J Chem Soc Chem Commun* 1979; 6: 288–289.
81. Huheey JE. The electronegativity of groups. *J Phys Chem* 1965; 69: 3284–3291.
82. Sierzputowska-Gracz H, Gopal HD and Agris PF. Comparative structural analysis of 1-methyladenosine, 7-methylguanosine, ethenoadenosine and their protonated salts IV: ^{1}H, ^{13}C, and ^{15}N NMR studies at natural isotope abundance. *Nucleic Acids Res* 1986; 14: 7783–7801.
83. Yamagata Y, Fukumoto S, Hamada K, et al. A novel guanine-guanine base pairing: crystal structure of a complex between 7-methylguanosine and its iodide. *Nucleic Acids Res* 1983; 11: 6475–6486.
84. Dunbar RC, Berden G and Oomens J. How does a small peptide choose how to bind a metal ion? IRMPD and computational survey of CS versus iminol binding preferences. *Int J Mass Spectrom* 2013; 354–355: 356–364.
85. Drayß MK, Armentrout PB, Oomens J, et al. IR spectroscopy of cationized aliphatic amino acids: stability of charge-solvated structure increases with metal cation size. *Int J Mass Spectrom* 2010; 297: 18–27.
86. Drayß MK, Blunk D, Oomens J, et al. Gas-phase structures of solution-phase zwitterions: charge solvation or salt bridge? *Int J Mass Spectrom* 2009; 281: 97–100.
87. Dunbar RC, Polfer NC and Oomens J. Gas-phase zwitterion stabilization by a metal dication. *J Am Chem Soc* 2007; 129: 14562–14563.
88. Citir M, Stennett EMS, Oomens J, et al. Infrared multiple photon dissociation spectroscopy of cationized cysteine: effects of metal cation size on gas-phase conformation. *Int J Mass Spectrom* 2010; 297: 9–17.
89. Armentrout PB, Rodgers MT, Oomens J, et al. Infrared multiphoton dissociation spectroscopy of cationized serine: effects of alkali-metal cation size on gas-phase conformation. *J Phys Chem A* 2008; 112: 2248–2257.
90. Forbes MW, Bush MF, Polfer NC, et al. Infrared spectroscopy of arginine cation complexes: direct observation of gas-phase zwitterions. *J Phys Chem A* 2007; 111: 11759–11770.
91. Bush MF, Oomens J, Saykally RJ, et al. Effects of alkaline Earth metal ion complexation on amino acid zwitterion stability: results from infrared action spectroscopy. *J Am Chem Soc* 2008; 130: 6463–6471.
92. Gelbin A, Schneider B, Clowney L, et al. Geometric parameters in nucleic acids: sugar and phosphate constituents. *J Am Chem Soc* 1996; 118: 519–529.
93. Davies DB and Danyluk SS. Nuclear magnetic resonance studies of 5′-ribo-and deoxyribonucleotide structures in solution. *Biochemistry* 1974; 13: 4417–4434.
94. Podolyan Y, Gorb L and Leszczynski J. Protonation of nucleic acid bases. A comprehensive Post-Hartree–Fock study of the energetics and proton affinities. *J Phys Chem A* 2000; 104: 7346–7352.
95. Hunter EP and Lias SG. Evaluated gas phase basicities and proton affinities of molecules: an update. *J Phys Chem Ref Data* 1998; 27: 413–656.
96. Greco F, Liguori A, Sindona G, et al. Gas-phase proton affinity of deoxyribonucleosides and related nucleobases by fast atom bombardment tandem mass spectrometry. *J Am Chem Soc* 1990; 112: 9092–9096.
97. Russo N, Toscano M, Grand A, et al. Protonation of thymine, cytosine, adenine, and guanine DNA nucleic acid bases: theoretical investigation into the framework of density functional theory. *J Comput Chem* 1998; 19: 989–1000.
98. Chandra AK, Nguyen MT, Uchimaru T, et al. Protonation and deprotonation enthalpies of guanine and adenine and implications for the structure and energy of their complexes with water: comparison with uracil, thymine, and cytosine. *J Phys Chem A* 1999; 103: 8853–8860.
99. Moser A, Range K and York DM. Accurate proton affinity and gas-phase basicity values for molecules important in biocatalysis. *J Phys Chem B* 2010; 114: 13911–13921.